Article

Discovery Medicine 2026; 38(206): 715–731
https://doi.org/10.24976/Discov.Med.202638206.59

Small Intestinal Enteroendocrine Cell-Derived Exosomes Inhibit Endoplasmic Reticulum Stress-Induced Ferroptosis in Pancreatic β-Cells

Xiaoxi Chen[1], Lin Huang[1], Xiaoyan Zhu[2,*]

[1]Department of Gastroenterology, Affiliated Maternity and Child Health Care Hospital of Nantong University, 226001 Nantong, Jiangsu, China
[2]Department of Endocrinology, Affiliated Maternity and Child Health Care Hospital of Nantong University, 226001 Nantong, Jiangsu, China
*Correspondence: xiaoyan15951303862@163.com (Xiaoyan Zhu)
Submitted: 23 September 2025 Revised: 26 November 2025 Accepted: 10 December 2025 Published: 20 March 2026

Background: Type 2 diabetes mellitus (T2DM) is driven by progressive β-cell failure, wherein endoplasmic reticulum (ER) stress activates the Protein kinase R-Like ER kinase (PERK)-activating transcription factor 4 (ATF4) signaling cascade, promoting ferroptosis and accelerating β-cell dysfunction. This study investigated whether STC-1–derived exosomes (EXO) protect β-cells by modulating this pathway.

Methods: A T2DM mouse model was induced via high-fat diet (HFD) feeding and streptozotocin (STZ) administration. Exosomes were extracted from STC-1 cell culture supernatants, followed by both *in vitro* cellular experiments and *in vivo* animal studies. MIN6 cells cultured under high-glucose (HG) conditions were treated with graded concentrations of STC-1-EXO or the ferroptosis inhibitor Ferrostatin-1. Cell viability was quantified using cell Counting Kit-8 (CCK-8) assay. Western blotting (WB) assessed expression of ferroptosis markers acyl-CoA synthetase long-chain family member 4 (ACSL4) and glutathione peroxidase 4 (GPX4). Ferroptotic activity was evaluated by measuring intracellular total iron concentration, malondialdehyde (MDA) content, and glutathione (GSH) levels. *In vivo*, T2DM mice received STC-1-EXO treatment, followed by assessment of random blood glucose, glucose tolerance, insulin sensitivity, and pancreatic histopathology with concomitant protein expression analysis.

Results: *In vitro*, STC-1-EXO dose-dependently reversed HG-induced MIN6 cell viability loss ($p < 0.05$). Relative to the high-glucose control group, STC-1-EXO treatment significantly attenuated intracellular iron accumulation and MDA production, while restoring GSH levels and reducing lipid peroxidation ($p < 0.05$). WB results revealed that compared to the HG group, STC-1-EXO treatment significantly downregulated the expression of ER stress markers glucose-regulated protein 78 (GRP78), phosphorylated-PERK (p-PERK), phosphorylated eukaryotic translation initiation factor 2α (p-eIF2α), and ATF4, while simultaneously reducing the pro-ferroptotic protein ACSL4 expression and increasing the anti-ferroptotic protein GPX4 expression ($p < 0.05$). *In vivo* experiments showed that compared to untreated T2DM mice, STC-1-EXO-treated mice exhibited significantly decreased random blood glucose levels and markedly improved glucose tolerance and insulin sensitivity ($p < 0.05$). Hematoxylin and Eosin (H&E) staining revealed increased islet area and enhanced β-cell numbers in STC-1-EXO-treated mice. Furthermore, compared to untreated T2DM mice, STC-1-EXO treatment significantly reduced the expression of GRP78, p-PERK, p-eIF2α, and ATF4 in pancreatic tissue, decreased ACSL4 expression while increasing GPX4 expression, and resulted in significantly decreased MDA levels and elevated GSH levels in pancreatic tissue ($p < 0.05$).

Conclusion: STC-1-EXO effectively ameliorates ER stress and ferroptosis in pancreatic β-cells through inhibition of the PERK-ATF4 signaling pathway, thereby improving blood glucose levels and insulin secretory function in T2DM mice. This finding provides a novel theoretical foundation and potential therapeutic strategies for exosome-based diabetes treatment.

Keywords: type 2 diabetes mellitus; small intestinal enteroendocrine cells; exosomes; pancreatic β-cells; ferroptosis; endoplasmic reticulum stress

Introduction

With the transformation of lifestyle patterns and the acceleration of population aging processes, type 2 diabetes mellitus (T2DM) has emerged as one of the most severe chronic non-communicable diseases threatening human health globally [1]. According to the International Diabetes Federation (IDF) statistics, approximately 463 million adults worldwide were afflicted with diabetes in 2019, with over 90% representing T2DM patients. The incidence rate demonstrates an annually ascending trajectory, particularly pronounced in developing nations [2].

The fundamental pathophysiological mechanisms underlying T2DM center on the progressive deterioration of pancreatic β-cell function coupled with peripheral tissue insulin resistance, resulting in relative or absolute insulin

secretion insufficiency and consequent sustained hyperglycemic states [3,4]. Chronic hyperglycemic conditions can precipitate a cascade of complications, including cardiovascular diseases, nephropathy, retinopathy, and neuropathy, substantially compromising patients' quality of life [5]. While currently employed clinical hypoglycemic agents demonstrate certain efficacy in glycemic control, the majority fail to fundamentally ameliorate β-cell function. Furthermore, certain pharmacological interventions may induce adverse effects such as hypoglycemia, weight gain, and gastrointestinal discomfort, thereby constraining their long-term clinical application [6].

In recent years, the pivotal role of intercellular communication in regulating pancreatic β-cell function has garnered increasing academic attention. Among these mechanisms, exosomes, as novel intercellular information transfer vehicles, provide innovative therapeutic approaches and potential targets for T2DM treatment through their distinctive nanoscale architecture and enrichment with diverse bioactive molecules [7–10]. Exosomes represent minute vesicles secreted by cells, ubiquitously distributed across various bodily fluids, capable of transporting proteins, lipids, mRNA, and microRNA, thereby serving crucial functions in intercellular material exchange and signal transduction processes [11–13].

Small intestinal enteroendocrine cells (STC-1), as integral components of the gastrointestinal endocrine system, not only participate in regulating intestinal motility and digestive secretion but also influence glucose metabolism and pancreatic β-cell function through the secretion of various hormones and exosomes [14–16]. Preliminary investigations have demonstrated that STC-1 cell-derived exosomes (STC-1-EXO) exhibit considerable potential in ameliorating insulin resistance, promoting insulin secretion, and protecting pancreatic β-cells [17,18]. However, their specific mechanistic pathways remain incompletely elucidated.

Within cellular physiological processes, endoplasmic reticulum (ER) stress constitutes a prevalent pathological state, intimately associated with aberrant protein folding, intracellular calcium homeostasis dysregulation, and oxidative stress [19–21]. ER stress can induce ferroptosis through activation of multiple signaling cascades, including the RNA-dependent Protein kinase R-Like ER kinase (PERK)-activating transcription factor 4 (ATF4) pathway [22]. Ferroptosis represents a novel iron-dependent cell death modality characterized by intracellular iron metabolism disruption, intensified lipid peroxidation reactions, and compromised antioxidant defense system functionality [23]. In the pathogenesis and progression of T2DM, pancreatic β-cells are susceptible to the dual impacts of ER stress and ferroptosis, leading to progressive functional deterioration and ultimately resulting in insufficient insulin secretion [24].

Although current research has partially explored the therapeutic prospects of exosomes in diabetes treatment, comprehensive systematic investigations regarding whether STC-1-EXO can protect pancreatic β-cell function through regulating ER stress and ferroptosis remain notably absent from the literature. Therefore, this study aims to systematically investigate the effects of STC-1-EXO on pancreatic β-cell ferroptosis and elucidate its underlying mechanistic pathways, with particular emphasis on examining whether it inhibits ER stress through targeting the PERK-ATF4 pathway, thereby mitigating ferroptosis-mediated pancreatic β-cell damage. This research endeavors to provide novel theoretical foundations and potential therapeutic strategies for T2DM prevention and treatment.

Materials and Methods

Construction of Type 2 Diabetes Animal Model and Therapeutic Administration Protocol

Male C57BL/6J wild-type mice, aged 6 weeks and weighing 20 $\pm$ 2 g, were obtained from Beijing Vital River Laboratory Animal Technology Co., Ltd. (License Number: SCXK (Beijing) 2021-0011). After a 1-week acclimation period, mice were randomized assigned to three groups (n = 6 mice per group): control, type 2 diabetes mellitus (T2DM), and T2DM + exosome (EXO) treatment. All protocols were approved by the Institutional Animal Care and Use Committee of Nantong University (Approval Number: P20230321-018) and conducted in accordance with National Institutes of Health (NIH) guidelines.

The T2DM murine model was constructed following established methodological protocols described in previous literature [25]. In brief, T2DM was induced by feeding mice a high-fat diet (HFD, 60% fat content, Research Diets, New Brunswick, NJ, USA, D12492) for 12 weeks. At week 8, mice received tail-vein injections of streptozotocin (STZ, Sigma-Aldrich, St. Louis, MO, USA, S0130) at 60 mg/kg dissolved in 0.1 M sodium citrate buffer (pH = 4.5) for five consecutive days. Control group mice were fed standard chow and received equivalent volume injections of 0.1 M sodium citrate buffer (pH = 4.5). The criterion for successful model establishment was defined as fasting blood glucose levels $\geq$16.7 mmol/L.

STC-1-EXO (100 µg per mouse) were administered via tail vein injection twice weekly for 4 weeks (weeks 9–12, 8 total doses). Control group received equivalent volumes of phosphate-buffered saline (PBS).

Hematoxylin and Eosin Staining (H&E)

Mice were deeply anesthetized with 5% isoflurane until loss of corneal and pedal reflexes, then euthanized by cervical dislocation. Pancreata were immediately harvested and fixed in 10% neutral buffered formalin (Solarbio, Beijing, China, G2161) for 24 h. Tissues were processed through graded ethanol dehydration (70%, 75%, 80%, 85%, 90%, 95%, 100%), xylene clearing, and paraffin embedding. Serial sections (4 µm-thick) were mounted

on adhesive slides, baked at 60 °C for 2 h, dewaxed in xylene, and rehydrated. Histological staining was performed through 10 min hematoxylin solution (Solarbio, Beijing, China, G1150) immersion, followed by running water rinse to eliminate excess stain, and subsequent 5 min eosin solution (Solarbio, Beijing, China, G1100) staining. Final processing involved sequential gradient ethanol dehydration (50%, 70%, 80%, 90%, 100%), xylene clearing, and neutral resin mounting. Microscopic examination and photographic documentation were conducted using an optical microscope (Olympus BX53, Tokyo, Japan) for subsequent image analysis. Islet area was quantified using ImageJ v1.54i software (National Institutes of Health, Bethesda, MD, USA).

Random Blood Glucose Determination

Blood glucose measurements were performed using micro-capillary blood sampling from tail vein puncture, with glucose quantification conducted via Accu-Chek Performa glucometer (Roche Diagnostics GmbH, Mannheim, Germany, 13409711001). Measurement accuracy was ensured through standard calibration procedures prior to each assessment. Throughout the experimental period, fasting random blood glucose levels were monitored twice weekly, specifically conducted during Tuesday morning sessions (9:00–11:00) and Friday afternoon sessions (15:00–17:00). The mice were returned to ad libitum feeding immediately after each measurement.

Glucose-Stimulated Insulin Secretion (GSIS)

Following methodological protocols established by Xia *et al*. [25]. MIN6 cells were seeded at a density of 1×10^6 cells per well in 24-well culture plates, with subsequent group-specific treatment interventions applied following cellular adherence, and cultivation continued for 24 h. Experimental procedures involved initial 30 min pre-incubation with glucose-free KRBS-Ringer Bicarbonate (KRB) buffer to achieve glucose depletion, followed by incubation with 2.5 mmol/L glucose-containing KRB buffer for 1 h with supernatant collection. Subsequently, cells were incubated with 25 mmol/L glucose-containing KRB buffer for an additional hour, with final supernatant collection. Insulin concentrations in MIN6 cell culture supernatants were quantified using a mouse insulin ELISA detection kit (Finetest, Wuhan, China, EM0260).

Mouse Serum Insulin Determination, Intraperitoneal Glucose Tolerance Test (IPGTT), and Intraperitoneal Insulin Tolerance Test (IPITT)

IPGTT and IPITT procedures were conducted according to previously established methodological protocols [26]. For IPGTT assessment, mice underwent 16 h fasting followed by intraperitoneal administration of 1.5 g/kg glucose (Sigma-Aldrich, G7021). Blood samples were collected via tail-tip at baseline and at 15, 30, 60, 90, and 120 minutes post-injection for glycemic determination. For IPITT evaluation, mice were subjected to 4 h fasting prior to intraperitoneal injection of 0.75 U/kg insulin (Sigma-Aldrich, I5508). Blood glucose measurements were performed via tail-tip at identical temporal intervals as described for IPGTT. Quantitative analysis of IPGTT and IPITT data was performed using GraphPad Prism 9.5.0 software (GraphPad Software, San Diego, CA, USA). Serum samples were collected under fasting conditions and at 30 minutes post-IPGTT initiation from the inner canthus vein. Before blood was drawn from the inner canthal vein, the mice were deeply anesthetized by exposure to 5% isoflurane, followed by 2% maintenance. Serum insulin concentrations were quantified using a mouse insulin ELISA detection kit.

Cell Culture Methodology

STC-1 cells were procured from Zhejiang Meisen Cell Technology Co., Ltd., Hangzhou , China (CTCC-001-0254) and maintained in RPMI 1640 medium (Gibco, Waltham, MA, USA, 11875093) supplemented with 10% fetal bovine serum (FBS, Gibco, Waltham, MA, USA, 10099141), 100 U/mL penicillin, and 100 µg/mL streptomycin (Gibco, Waltham, MA, USA, 15140122). MIN6 cells were obtained from Shanghai EK-Bioscience Biotechnology Co., Ltd., Shanghai, China (CC-Y2103) and cultured in DMEM medium (Gibco, Waltham, MA, USA, 11885084) containing 15% FBS (Gibco, Waltham, MA, USA, 10099141), 1 mM sodium pyruvate (Sigma-Aldrich, St. Louis, MO, USA, P2256), 2mM L-glutamine (Gibco, Waltham, MA, USA, 25030081), and 50 µM β-mercaptoethanol (Sigma-Aldrich, St. Louis, MO, USA, M6145). Both cell lines were maintained under standardized culture conditions at 37 °C with 5% CO_2 atmosphere, with subcultivation performed every three days at a 1:3 ratio. MIN6 cells exhibited typical epithelial morphology with a polygonal shape and formed islet-like clusters at high confluence, consistent with pancreatic β-cells' characteristics. STC-1 cells displayed adherent epithelial morphology, appearing as polygonal or short spindle-shaped cells with relatively uniform size, consistent with intestinal enteroendocrine cell features. Both STC-1 and MIN6 cells were routinely tested for mycoplasma contamination and were confirmed to be mycoplasma-negative prior to use in all experiments.

Following previously established methodological approaches [25]. Hyperglycemic cellular models were constructed through glucose concentration-dependent MIN6 cell incubation. Third-passage MIN6 cells were utilized for experimental procedures, with high-glucose (HG) groups exposed to 33.3 mM glucose and control groups maintained at 5.5 mM glucose concentrations. Six independent experimental replicates were performed for each treatment group.

To systematically investigate ferroptosis and endoplasmic reticulum stress effects on MIN6 cells and elucidate underlying mechanistic pathways, experimental pro-

tocols incorporated ferroptosis agonist Erastin (HY-15763, Monmouth Junction, NJ, USA) and ferroptosis inhibitor Ferrostatin-1 (Fer-1, HY-100579, MCE, Monmouth Junction, NJ, USA), alongside PERK activator CCT020312 (HY-119240, Monmouth Junction, NJ, USA) and PERK inhibitor GSK2606414 (HY-18072, Monmouth Junction, NJ, USA). MIN6 cells were seeded at 5×10^5 cells per well in 6-well culture plates, with experimental treatments initiated upon achieving approximately 70% confluency. For ferroptosis-related investigations, cells underwent hyperglycemic cultivation with concurrent treatment of either 100 µg/mL STC-1-EXO or 10 µM Fer-1 for 24 h durations. To validate STC-1-EXO-mediated ferroptosis inhibition, selected experimental groups received co-treatment with 20 µM Erastin ferroptosis agonist alongside STC-1-EXO for 24 h. In PERK-ATF4 signaling pathway investigations, MIN6 cells were subjected to hyperglycemic conditions with 100 µg/mL STC-1-EXO treatment for 24 h, accompanied by either 5 µM PERK activator CCT020312 or 150 nM PERK inhibitor GSK2606414 to assess modulatory effects on STC-1-EXO functionality. All experimental interventions were administered on the second day post-seeding, with 24 h treatment durations followed by cellular harvest for subsequent analytical procedures.

Lentiviral Transfection Methodology

ATF4 overexpression lentiviral (LV) particles were employed for genetic manipulation experiments (plasmid sequence information is provided in **Supplementary Material**). MIN6 cells were seeded at 2×10^4 cells per well in 24-well plates. Then, MIN6 cells were infected at 20–30% confluence with ATF4 overexpression LV (5×10^5 TU, MOI of 50) in the presence of 8 µg/mL polybrene (Sigma-Aldrich, St. Louis, MO, USA, P4330). Vector control groups were transfected with empty-vector viral. After 72 h, green fluorescent protein (GFP) fluorescence was visualized to confirm infection, and ATF4 overexpression was verified by Western blot.

Exosome Isolation and Characterization

STC-1 cells were seeded at 2×10^6 cells per 10 cm culture dish, with medium replacement to serum-free RPMI 1640 upon achieving approximately 70% confluence, followed by 48 h cultivation for exosome-containing supernatant collection. Subsequent processing involved sequential differential centrifugation at 4 °C: 300 ×g for 10 minutes, 2000 ×g for 20 minutes, and 10,000 ×g for 30 minutes to eliminate cellular debris and large particulate matter. Supernatants were filtered through 0.22 µm membranes to remove bacterial contamination and residual large particles. Filtered supernatants were transferred to ultracentrifugation tubes for 120,000 ×g centrifugation at 4 °C for 70 minutes to pellet exosomes. Exosome pellets were gently resuspended in pre-chilled PBS and subjected to additional 120,000 ×g centrifugation for 70 minutes for further purification. Final exosome preparations were resuspended in minimal PBS volumes, aliquoted, and stored at –80 °C.

For exosome characterization, transmission electron microscopy (TEM) was employed for morphological assessment. Approximately 10 µL resuspended exosome samples were uniformly distributed onto copper grids, followed by 15 min fixation in 2.5% glutaraldehyde solution (Solarbio, Beijing, China, G1200), excess solution removal, and 5 min uranyl acetate staining. Following natural desiccation, processed grids were examined using TEM (Tecnai G2 Spirit, FEI, Hillsboro, OR, USA) for morphological and dimensional analysis with photographic documentation. Concurrent Western blotting analysis was performed to detect exosomal markers cluster of differentiation 9 (CD9) and cluster of differentiation 63 (CD63) expression, with cytochrome C serving as a negative control to confirm exosomal identity of isolated vesicles.

Exosome Internalization Assay

STC-1-EXO were labeled with Vybrant™ DiO cell-labeling solution (Invitrogen, Waltham, MA, USA, V22886) for 15 min at room temperature. Labeled exosomes were co-incubated with MIN6 cells for 24 h, with fluorescence intensity monitoring performed at 4 h intervals using fluorescence microscopy. DiO-labeled exosome internalization by MIN6 cells was visualized using fluorescence microscopy (Olympus BX53, excitation wavelength 484–501 nm) with photographic documentation of fluorescent signals.

CCK-8 Cell Viability Assay

Following 24 h co-incubation of varying STC-1-EXO concentrations (25, 50, 100, 200 µg/mL) with MIN6 cells, 10 µL CCK-8 solution (Yeasen, 40203ES76, China) was added per well for 1 h incubation at 37 °C. Absorbance measurements were performed at 450 nm wavelength using a microplate reader (BioTek, Epoch 2) for cell viability calculations. Cell viability was calculated as: $(OD_{experimental} - OD_{blank}) / (OD_{control} - OD_{blank}) \times 100\%$. OD values represent optical density (OD).

Mitochondrial and Endoplasmic Reticulum Morphological Analysis

MIN6 cells were seeded at 1×10^5 cells per well in 12-well culture plates, with experimental treatments administered upon achieving approximately 70% cellular confluence according to designated experimental groupings. Following specified treatment durations, cells were enzymatically dissociated using 0.25% EDTA-trypsin, centrifugally collected, and immediately subjected to fixation in 2.5% glutaraldehyde solution for approximately 2 h to ensure comprehensive preservation of cellular ultrastructural integrity. Subsequently, fixed specimens underwent sequential gradient ethanol dehydration (30%, 50%, 70%, 80%, 90%, 100%) with 15 min intervals per concentration to

achieve complete cellular dehydration, followed by dual acetone replacement procedures (15 minutes each) for optimal preparation. Cellular specimens were then embedded in epoxy resin and subjected to overnight polymerization at 60 °C. Ultrathin sectioning was performed using an ultramicrotome to generate approximately 70 nm sections, which were collected on 200-mesh copper grids. Sectioned specimens underwent sequential staining protocols: 10 min incubation in 2% uranyl acetate under light-protected conditions followed by triple ultrapure water rinses, subsequently treated with lead citrate solution for 10 minutes with additional triple washing procedures. Post-staining specimens were air-dried overnight at room temperature within copper grid storage systems. TEM examination was conducted using a Tecnai G2 Spirit (FEI) system operating at 80 kV acceleration voltage for comprehensive ultrastructural morphological assessment.

Total Cellular Iron Determination

Intracellular total iron concentrations in MIN6 cells were quantified utilizing an iron detection kit (Solarbio, Beijing, China, BC5315) according to manufacturer's specifications. Cellular lysates were combined with kit working solutions, incubated at 37 °C for 15 minutes, followed by spectrophotometric absorbance measurements at 532 nm wavelength using a microplate reader. Iron content was calculated from a standard curve.

Lipid Peroxidation Assessment

Lipid peroxidation analysis in MIN6 cells was performed using the Liperfluo staining kit (Dojindo Molecular Technologies Inc., Kumamoto, Japan, L248). MIN6 cells were seeded at 1×10^5 cells per well in 24-well plates with subsequent treatment administration. Post-treatment specimens received 10 µM Liperfluo dye supplementation followed by 30 min incubation at 37 °C under light-protected conditions. Following triple PBS washing procedures, fluorescence microscopy examination (Olympus BX53, Tokyo, Japan, excitation wavelength 488 nm) was conducted for image capture. The fluorescence intensity was quantified with Image J software (v1.54i, NIH, Bethesda, MD, USA).

Malondialdehyde (MDA) and Glutathione (GSH) Detection

Cellular and pancreatic tissue MDA concentrations were determined using a lipid peroxidation MDA detection kit (Nanjing Jiancheng Bioengineering Institute, Nanjing, China, A003-1-2). Following manufacturer's protocols, cellular or tissue lysates were combined with thiobarbituric acid reagent, subjected to 95 °C water bath heating for 45 minutes, cooled to room temperature, and spectrophotometrically analyzed at 532 nm wavelength for MDA content calculation via standard curve methodology. Intracellular GSH levels were quantified using a GSH detection kit (Nanjing Jiancheng Bioengineering Institute, Nanjing, China, A006-2-1). Cellular lysates were combined with detection working solutions, incubated at 37 °C for 15 minutes, followed by absorbance measurement at 405 nm wavelength with GSH content determination through standard curve analysis.

Western Blotting

Total protein extraction from MIN6 cells and pancreatic tissues was performed using RIPA lysis buffer (Beyotime, Beijing, China, P0013) supplemented with protease and phosphatase inhibitor cocktails. Protein concentrations were determined using the BCA protein assay kit (Beyotime, Beijing, China, P0012). Protein samples were combined with loading buffer, denatured at 100 °C for 5 minutes, and subjected to 10% SDS-PAGE electrophoretic separation. Following electrophoresis, proteins were transferred to PVDF membranes (Millipore, Burlington, MA, USA, IPVH00010) and blocked with 5% non-fat milk solution for 1 hour. Primary antibody incubations were performed overnight at 4 °C using the following antibodies: glucose-regulated protein 78 (GRP78), (Proteintech, Wuhan, China, 11587-1-AP, 1:2000), p-PERK (Proteintech, Wuhan, China, 29546-1-AP, 1:1000), PERK (Abcam, Cambridge, UK, ab229912, 1:1000), p-eIF2α (CST, Danvers, MA, USA, #3398, 1:500), eIF2α (CST, Danvers, MA, USA, #5324, 1:1000), ATF4 (Proteintech, Wuhan, China, 10835-1-AP, 1:1000), acyl-CoA synthetase long-chain family member 4 (ACSL4) (Abcam, Cambridge, UK, ab155282, 1:1000), glutathione peroxidase 4 (GPX4) (Abcam, Cambridge, UK, ab125066, 1:1000), CD63 (CST, Danvers, MA, USA, #10112, 1:1000), CD9 (CST, Danvers, MA, USA, #98327, 1:1000), cytochrome C (CST, Danvers, MA, USA, #11940, 1:1000), and β-actin (Proteintech, Wuhan, China, 20536-1-AP, 1:1000). Subsequently, membranes were incubated with appropriate HRP-conjugated secondary antibodies (Proteintech, Wuhan, China, SA00001-2, 1:5000) for 1 hour at room temperature. Protein detection was accomplished using enhanced chemiluminescence reagent (Millipore, Burlington, MA, USA, WBKLS0100) with image acquisition performed via gel documentation system (Tanon 5200, Shanghai, China). Densitometric analysis of protein bands was conducted using ImageJ software for quantitative assessment.

Statistical Analysis

All experimental data are presented as mean $\pm$ standard deviation (mean $\pm$ SD). Statistical analyses were performed using GraphPad Prism 9.5.0 software. Normality was assessed using the Shapiro-Wilk test. For normally distributed data, Intergroup comparisons were conducted using one-way analysis of variance (One-way ANOVA) followed by Tukey's post-hoc test as appropriate for experimental design. For insulin-release assays, IPGTT, IPITT, body weight and random glucose measurements,

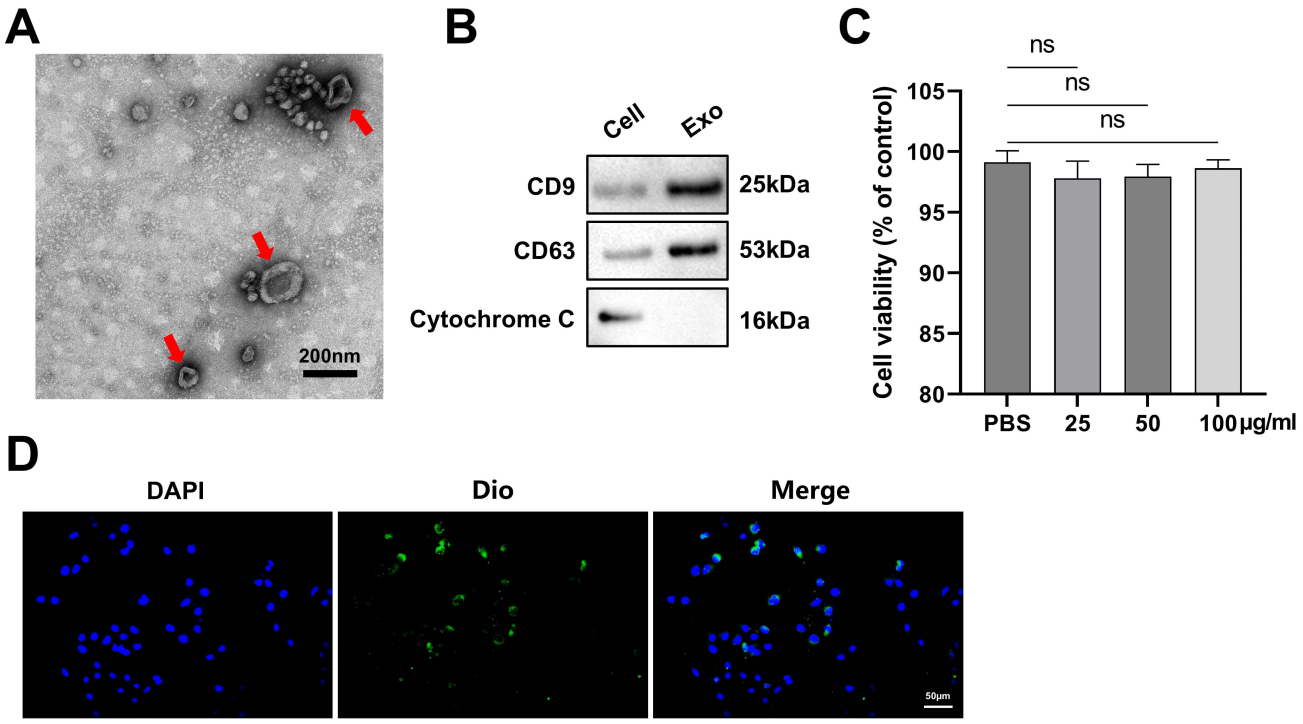

Fig. 1. Characterization and cellular internalization of STC-1 cell-derived exosomes. (A) TEM images of purified STC-1 cell-derived exosomes. Scale bar, 200 nm. The red arrows indicate exosomes. (B) WB analysis demonstrating expression levels of exosomal markers CD63 and CD9, alongside cell-specific marker cytochrome C in isolated STC-1-EXO preparations. (C) Cell viability assessment of MIN6 β-cells following 24 h treatment with varying concentrations (0, 25, 50, 100 μg/mL) of STC-1 cell-derived exosomes, evaluated using CCK-8 assay. Control groups received equivalent volume PBS treatment. (D) Representative fluorescence microscopy images of Dio-labeled STC-1-EXO internalization within MIN6 cells following 24 h co-incubation with Dio dye-labeled exosomes. Scale bar, 50 μm. Data are presented as mean ± standard deviation (mean ± SD). n = 6 independent experiments. Statistical analysis was performed using one-way analysis of variance. ns, not significant. Abbreviations: CD9, cluster of differentiation 9; CD63, cluster of differentiation 63; STC-1, small intestinal enteroendocrine cells; TEM, transmission electron microscopy; WB, Western blotting; STC-1-EXO, STC-1 cell-derived exosomes; CCK-8, Cell Counting Kit-8; PBS, phosphate-buffered saline.

two-way analysis of variance (Two-way ANOVA) followed by Tukey's post-hoc test was used. Statistical significance was defined as $p < 0.05$.

Results

Characterization and Cellular Internalization of STC-1 Cell-Derived Exosomes

Initially, we successfully isolated exosomes (STC-1-EXO) from STC-1 cell culture supernatants through systematic purification protocols. TEM examination revealed that STC-1-EXO exhibited characteristic cup-shaped morphological configurations with particle dimensions ranging from approximately 100–150 nm (Fig. 1A). WB analysis demonstrated that the isolated STC-1-EXO expressed distinctive exosomal marker proteins CD9 and CD63, while exhibiting absence of cell-specific marker cytochrome C expression (Fig. 1B), thereby confirming the authenticity and purity of the isolated exosomal preparations.

Subsequently, we systematically investigated the effects of varying STC-1-EXO concentrations (25, 50, 100 μg/mL) on MIN6 cellular viability under physiological conditions. Following 24 h co-incubation with MIN6 cells, CCK-8 assay results demonstrated that compared to PBS-treated control groups, STC-1-EXO treatment did not significantly compromise MIN6 cellular viability ($p > 0.05$; Fig. 1C), indicating biocompatibility and absence of cytotoxic effects under experimental conditions. Furthermore, fluorescence microscopy examination following co-incubation of Dio-labeled STC-1-EXO with MIN6 cells revealed efficient exosomal internalization by MIN6 cells (Fig. 1D), providing evidence for effective cellular uptake and utilization of STC-1-EXO by pancreatic β-cells.

STC-1-EXO Inhibits High Glucose-Induced Ferroptosis in MIN6 Cells In Vitro

Given that hyperglycemia-induced oxidative stress-mediated ferroptosis constitutes a fundamental pathophysiological mechanism in diabetic progression [27,28]. We investigated whether STC-1-EXO modulates ferroptotic processes within diabetic pathological contexts. MIN6 cells were subjected to hyperglycemic culture conditions with

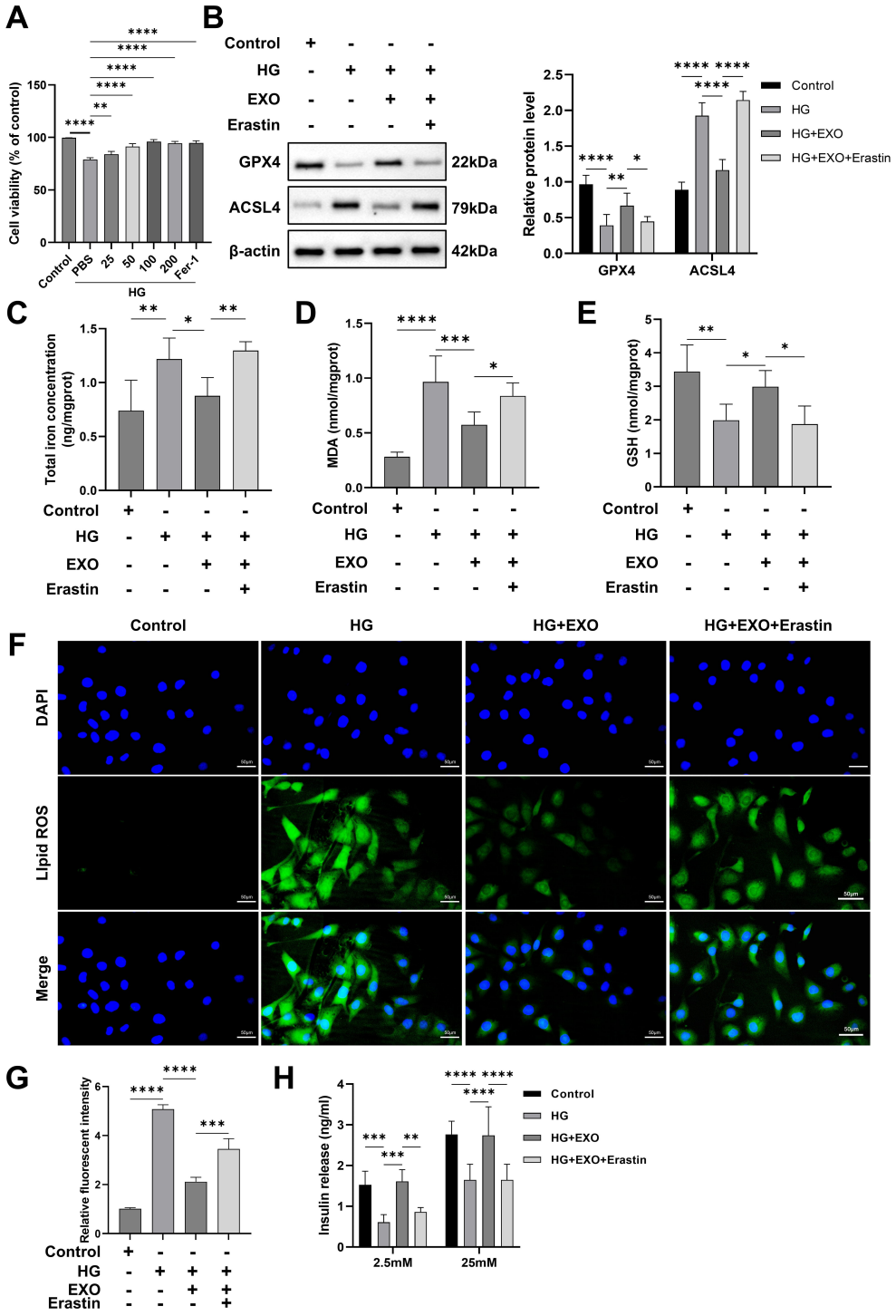

Fig. 2. STC-1-EXO inhibits high glucose-induced ferroptosis in MIN6 cells *in vitro*. (A) CCK-8 assessment of MIN6 cellular viability under hyperglycemic incubation conditions with varying exosome concentrations (25, 50, 100, 200 μg/mL) or ferroptosis inhibitor Fer-1 (10 μM) interventions. (B) WB detection of ferroptosis markers GPX4 and ACSL4. (C) Quantitative determination of total iron concentrations in MIN6 cells. (D) Quantitative measurement of MDA levels in MIN6 cells using MDA detection kit. (E) Quantitative assessment of GSH levels in MIN6 cells using GSH detection kit. (F,G) Detection of lipid peroxidation product content in MIN6 cells through Liperfluo staining methodology. Scale bar, 50 μm. (H) GSIS experimental evaluation of insulin release in MIN6 cells following 24 h treatment with ferroptosis agonist Erastin (20 μM). Data are presented as mean ± standard deviation (mean ± SD). n = 6 independent experiments. Statistical analysis performed using one-way analysis of variance. *$p < 0.05$, **$p < 0.01$, ***$p < 0.001$, ****$p < 0.0001$. Abbreviations: GPX4, glutathione peroxidase 4; ACSL4, acyl-CoA synthetase long-chain family member 4; EXO, exosomes; HG, high-glucose; Fer-1, Ferrostatin-1; MDA, malondialdehyde; GSH, glutathione; GSIS, Glucose-stimulated insulin secretion.

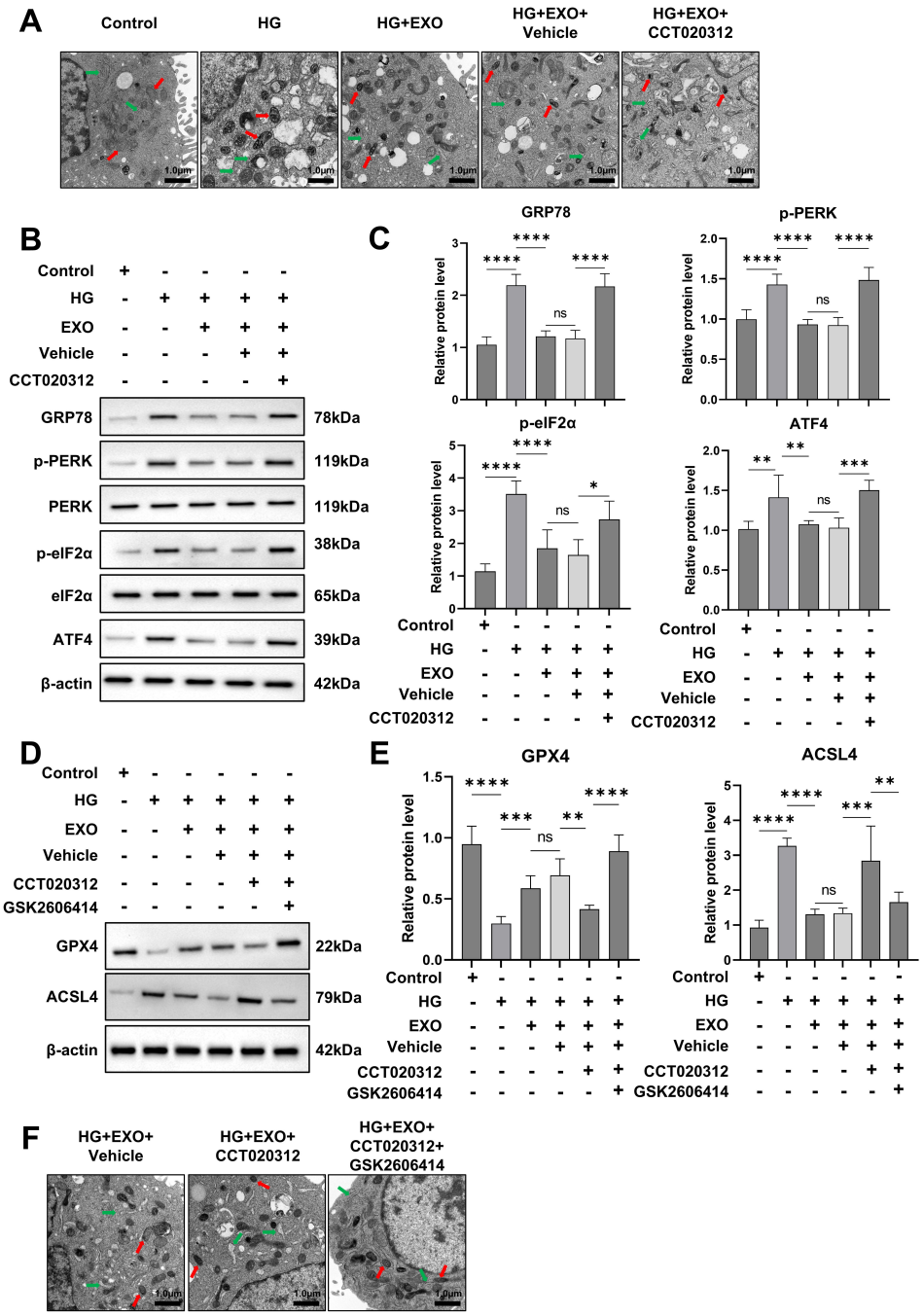

Fig. 3. PERK-ATF4 signaling pathway mediates STC-1-EXO's anti-ferroptotic effects in MIN6 cells. (A) TEM examination of mitochondrial and endoplasmic reticulum ultrastructure across experimental groups of MIN6 cells. Red arrows indicate mitochondria. Green arrows indicate endoplasmic reticulum. Scale bar = 1.0 μm. (B,C) WB analysis of GRP78, p-PERK, p-eIF2α, and ATF4 protein expression in MIN6 cells (B), with corresponding quantitative protein analysis (C). MIN6 cells were incubated for 24 h with or without PERK activator CCT020312 (5 μM). (D,E) Expression levels of ACSL4 and GPX4 proteins in MIN6 cells (D), with corresponding quantitative protein analysis (E). MIN6 cells were incubated for 24 h with or without CCT020312 (5 μM) and PERK inhibitor GSK2606414 (150 nM), followed by cellular harvest for WB analysis. (F) TEM examination of mitochondrial and endoplasmic reticulum structural architecture across experimental groups of MIN6 cells. Red arrows indicate mitochondria. Green arrows indicate endoplasmic reticulum. Scale bar = 1.0 μm. Data are presented as mean ± SD. n = 6 independent experiments per group. Statistical analysis was performed using one-way analysis of variance. *$p < 0.05$, **$p < 0.01$, ***$p < 0.001$, ****$p < 0.0001$. ns, not significant. Abbreviations: GRP78, glucose-regulated protein 78; p-PERK, phosphorylated-Protein Kinase RNA-like Endoplasmic Reticulum Kinase; p-eIF2α, phosphorylated eukaryotic translation initiation factor 2α; ATF4, activating transcription factor 4; GPX4, glutathione peroxidase 4; ACSL4, acyl-CoA synthetase long-chain family member 4; EXO, exosomes; HG, high glucose.

concurrent administration of varying STC-1-EXO concentrations (25, 50, 100, 200 µg/mL). CCK-8 analytical results demonstrated that hyperglycemic conditions alone significantly suppressed MIN6 cellular viability compared to control groups, whereas STC-1-EXO therapeutic intervention substantially restored cellular viability parameters ($p < 0.05$; Fig. 2A). The 100 µg/mL concentration group exhibited MIN6 cellular viability levels comparable to normal control groups, establishing this dosage as the reference concentration for subsequent experimental protocols ($p < 0.05$; Fig. 2A). Notably, hyperglycemic conditions combined with ferroptosis inhibitor Ferrostatin-1 (Fer-1) treatment resulted in marked elevation of MIN6 cellular viability compared to control groups ($p < 0.05$; Fig. 2A).

WB analysis revealed that compared to hyperglycemic treatment alone, hyperglycemia combined with STC-1-EXO significantly downregulated pro-ferroptotic protein ACSL4 expression while substantially enhancing anti-ferroptotic protein GPX4 expression levels ($p < 0.05$; Fig. 2B). However, the inhibitory effects of STC-1-EXO on hyperglycemia-induced ferroptosis were reversed by ferroptosis agonist Erastin administration, providing evidence for STC-1-EXO's regulatory involvement in ferroptotic pathways.

Comprehensive biochemical analysis demonstrated that STC-1-EXO treatment significantly reduced intracellular total iron concentrations ($p < 0.05$; Fig. 2C) and MDA expression levels ($p < 0.05$; Fig. 2D), while substantially elevating GSH expression levels ($p < 0.05$; Fig. 2E) in MIN6 cells. Concurrently, Liperfluo staining results revealed that STC-1-EXO markedly attenuated lipid peroxidation product accumulation within MIN6 cells compared to hyperglycemic treatment alone ($p < 0.05$; Fig. 2F,G). These findings demonstrate that STC-1-EXO effectively inhibits hyperglycemia-induced ferroptosis in MIN6 cells through multiple molecular mechanisms.

Finally, we systematically evaluated STC-1-EXO's effects on pancreatic β-cell functional parameters. Glucose-stimulated insulin secretion (GSIS) analysis demonstrated that hyperglycemia combined with STC-1-EXO treatment significantly enhanced MIN6 cellular insulin secretory capacity compared to hyperglycemic treatment groups ($p < 0.05$; Fig. 2H). These results establish that STC-1-EXO not only effectively inhibits hyperglycemia-induced MIN6 cellular ferroptosis but also improves insulin secretory functionality.

PERK-ATF4 Signaling Pathway Mediates STC-1-EXO's Anti-Ferroptotic Effects in MIN6 Cells

To elucidate the specific mechanistic pathways underlying STC-1-EXO's anti-ferroptotic properties, we conducted comprehensive ultrastructural analysis. Ferroptotic processes are characteristically accompanied by distinctive alterations in mitochondrial ultrastructural architecture. Through transmission electron microscopic examination of hyperglycemia-treated MIN6 cells, we observed substantial morphological modifications in both mitochondrial configurations and endoplasmic reticulum (ER) architecture. Given that previous research has established correlations between ER stress and oxidative stress phenomena, wherein ER stress activation can induce ferroptotic cell death through regulatory pathways such as PERK-ATF4 signaling cascades [29]. We hypothesized that ER stress constitutes a fundamental regulatory component in STC-1-EXO-mediated ferroptotic modulation within MIN6 cellular systems.

Transmission electron microscopic analysis revealed that control group MIN6 cells exhibited characteristic ER morphology consisting of parallel-arranged, flattened vesicular structures with well-preserved lamellar folded tubular configurations, alongside intact mitochondrial outer membranes with clearly delineated cristae structures. In contrast to control groups, hyperglycemic treatment groups displayed aberrant ER morphological characteristics, including expansion, vacuolization, and disappearance of lamellar folded tubular structures, accompanied by mitochondrial swelling and cristae obscuration. Within HG+EXO and HG+EXO+Vehicle treatment groups, exosomal therapeutic intervention substantially restored MIN6 cellular ER and mitochondrial ultrastructural architecture, manifesting as reduced ER expansion severity and normalized mitochondrial morphology. However, CCT020312 administration reversed exosomal therapeutic effects, with HG+EXO+CCT020312 groups exhibiting cellular ER expansion, vacuolization, and mitochondrial swelling with cristae obscuration (Fig. 3A).

WB analysis of hyperglycemia-incubated MIN6 cells demonstrated that compared to control groups, HG treatment significantly upregulated ER stress-associated protein expression levels, including GRP78, p-PERK, p-eIF2α, and ATF4 ($p < 0.05$; Fig. 3B,C). Following STC-1-EXO therapeutic intervention, protein expression levels of these ER stress markers in MIN6 cells were substantially reduced compared to HG treatment groups ($p < 0.05$; Fig. 3B,C). However, PERK activator CCT020312 administration compromised STC-1-EXO's anti-ER stress effects within hyperglycemic MIN6 cellular models ($p < 0.05$; Fig. 3B,C). These results indicate that ER stress is vital to STC-1-EXO-mediated cellular protection.

Subsequently, we investigated whether STC-1-EXO inhibits hyperglycemia-induced MIN6 cellular ferroptosis through ER stress pathway modulation. Following CCT020312 intervention in hyperglycemia-treated MIN6 cells, we determined that PERK activation reversed STC-1-EXO's modulatory effects on MIN6 cellular ACSL4 and GPX4 protein expression patterns. Specifically, compared to HG+EXO and HG+EXO+Vehicle groups, CCT020312-mediated ER stress activation resulted in elevated ACSL4 protein expression and decreased GPX4 protein expression ($p < 0.05$; Fig. 3D,E). Conversely, com-

pared to HG+EXO+CCT020312 groups, GSK2606414-mediated ER stress inhibition resulted in downregulated ACSL4 protein expression levels and upregulated GPX4 protein expression levels ($p < 0.05$; Fig. 3D,E).

Transmission electron microscopic results provided additional confirmatory evidence supporting our theoretical framework. Consistent with previous findings, compared to HG+EXO+Vehicle groups, HG+EXO+CCT020312 treatment groups exhibited disappearance of normal ER lamellar folded tubular structures, accompanied by mitochondrial swelling and cristae elimination ($p < 0.05$; Fig. 3F). Following PERK inhibitor GSK2606414 treatment of MIN6 cells, HG+EXO+GSK2606414 groups demonstrated improved cellular ER and mitochondrial morphology compared to HG+EXO+CCT020312 groups (Fig. 3F).

These experimental data demonstrate that STC-1-EXO prevents hyperglycemia-induced MIN6 cellular ferroptotic progression through PERK-ATF4 pathway inhibition and consequent ER stress attenuation.

ATF4 Overexpression Compromises STC-1-EXO's Protective Effects Against High Glucose-Induced Ferroptosis in MIN6 Cells

To systematically validate ATF4's fundamental importance in mediating STC-1-EXO's anti-ferroptotic therapeutic mechanisms, we employed lentiviral (LV) particles harboring ATF4 genetic constructs for MIN6 cellular transfection, successfully achieving robust ATF4 overexpression profiles (Fig. 4A). Within ATF4 overexpression experimental paradigms, STC-1-EXO's regulatory modulation of GPX4 and ACSL4 expression patterns was substantially attenuated, establishing mechanistic correlations between transcriptional factor activity and exosomal therapeutic efficacy.

Specifically, comparative analysis with Vector control groups demonstrated that ATF4 overexpression significantly downregulated GPX4 protein expression levels while concurrently upregulating ACSL4 protein expression levels ($p < 0.05$; Fig. 4B,C). Furthermore, lipid peroxidation assessment revealed that STC-1-EXO's inhibitory effects on lipid peroxidation product accumulation were markedly diminished within ATF4 overexpression cellular contexts (Fig. 4D,E).

These experimental findings establish ATF4's pivotal regulatory function within STC-1-EXO-mediated ferroptotic modulation processes and provide direct evidence supporting the theoretical framework wherein STC-1-EXO exerts anti-ferroptotic protective effects through systematic ATF4 inhibition.

STC-1-EXO Attenuates Endoplasmic Reticulum Stress and Ferroptosis in Pancreatic Tissues of T2DM Mice

To systematically evaluate the *in vivo* therapeutic efficacy of STC-1-EXO within established pathophysiological contexts, we constructed a comprehensive T2DM murine model through 12-week HFD administration combined with consecutive 5-day intravenous STZ injections, followed by 4-week therapeutic intervention involving bi-weekly tail vein STC-1-EXO administrations (Fig. 5A).

Within the established T2DM murine model framework, comparative analysis demonstrated that STC-1-EXO therapeutic intervention significantly attenuated pancreatic tissue expression levels of ER stress-associated proteins, including GRP78, p-PERK, p-eIF2α, and ATF4, relative to T2DM control groups ($p < 0.05$; Fig. 5B,C). Concurrently, exosomal treatment substantially reduced ACSL4 protein expression levels while enhancing GPX4 protein expression levels ($p < 0.05$; Fig. 5D,E), establishing a molecular signature consistent with ferroptotic pathway inhibition.

Furthermore, biochemical analysis revealed that T2DM+EXO treatment groups exhibited significantly decreased pancreatic tissue MDA levels coupled with elevated GSH concentrations compared to T2DM control groups ($p < 0.05$; Fig. 5F,G). These findings provide evidence that STC-1-EXO demonstrates *in vivo* therapeutic efficacy through systematic inhibition of both ER stress and ferroptotic pathways, thereby establishing a protective framework for pancreatic tissue preservation within diabetic pathophysiological contexts.

Early Preventive Treatment With STC-1-EXO Improves β-Cell Function in T2DM Mice

In the T2DM mouse model, early preventive treatment with STC-1-EXO demonstrated therapeutic efficacy across multiple metabolic parameters. At week 1, random blood glucose in the T2DM+EXO group was slightly reduced compared with the T2DM group, but the difference was not statistically significant. From week 2 onward until the end of the experiment, random blood glucose levels in the T2DM+EXO group remained significantly lower than those in the T2DM group ($p < 0.05$; Fig. 6A). Concurrently, STC-1-EXO treatment attenuated the declining trend in body weight, with some mice exhibiting weight recovery ($p < 0.05$; Fig. 6B).

IPGTT results demonstrated that glucose tolerance in the T2DM+EXO group was markedly superior to that observed in the T2DM group ($p < 0.05$; Fig. 6C,D). Similarly, IPITT results indicated that insulin sensitivity in the T2DM+EXO group was improved compared to the T2DM group ($p < 0.05$; Fig. 6E,F). GSIS experimental analysis revealed that compared to the T2DM group, STC-1-EXO treatment enhanced insulin secretory capacity in T2DM mice ($p < 0.05$; Fig. 6G). These findings demonstrate that STC-1-EXO not only reduces blood glucose levels but also improves glucose tolerance and insulin sensitivity, thereby ameliorating diabetic symptomatology.

Finally, H&E staining analysis revealed that compared to the T2DM group, STC-1-EXO treatment group mice exhibited increased pancreatic islet area ($p < 0.05$; Fig. 6H,I).

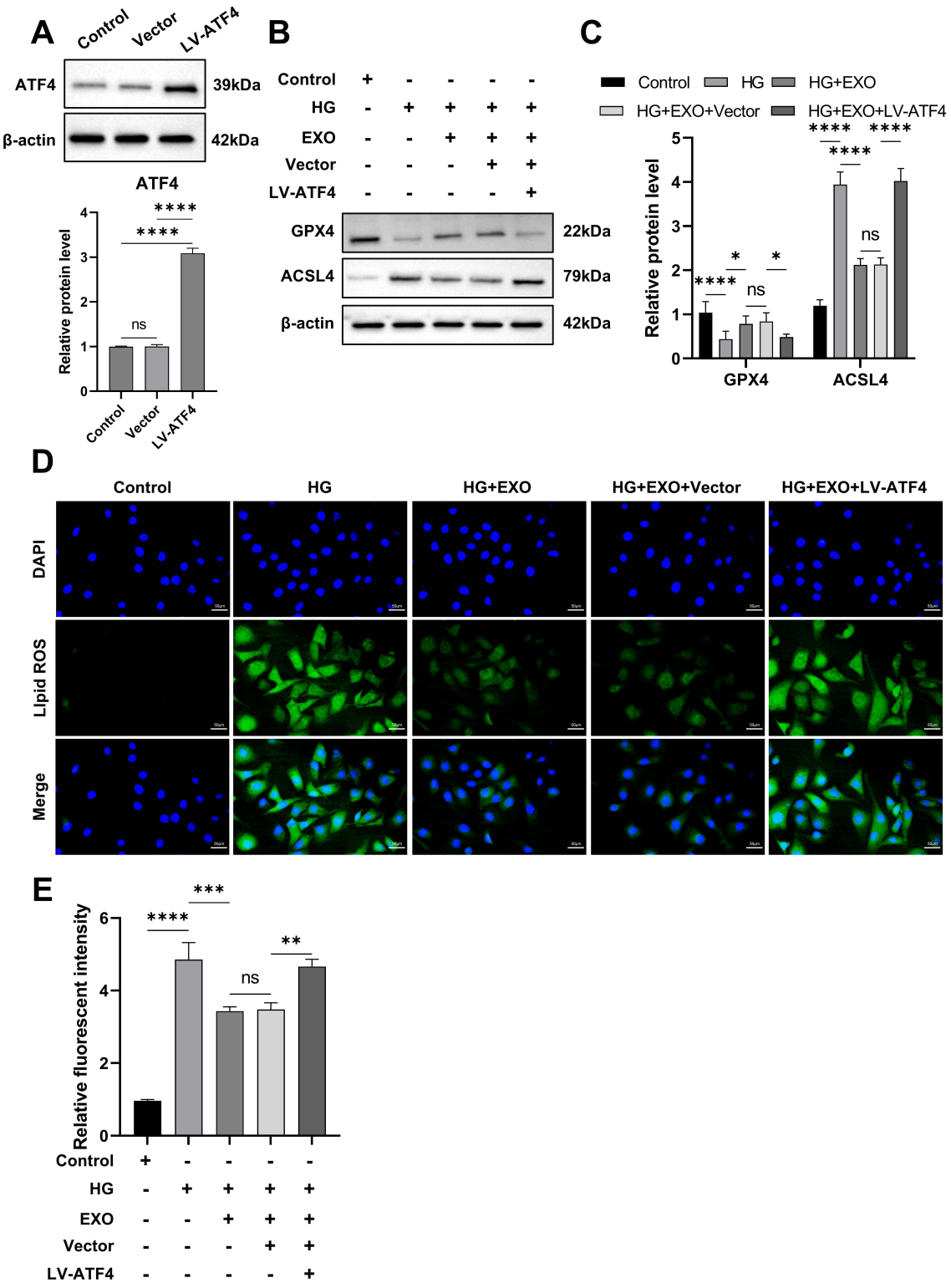

Fig. 4. ATF4 overexpression compromises STC-1-EXO's protective effects against high glucose-induced ferroptosis in MIN6 cells. (A) MIN6 cells were transfected with lentiviral particles carrying ATF4 genetic constructs, followed by WB assessment of ATF4 protein overexpression status. Blank control groups received no treatment intervention, while Vector control groups were transfected with empty vector control viral particles. (B,C) WB detection of ferroptosis markers GPX4 and ACSL4 (B), with corresponding quantitative protein analysis (C). (D,E) Detection of lipid peroxidation product content in MIN6 cells using Liperfluo staining methodology. Scale bar, 50 μm. Data are presented as mean ± SD. n = 6 independent experiments. Statistical analysis was performed using one-way analysis of variance. *$p < 0.05$, **$p < 0.01$, ***$p < 0.001$, ****$p < 0.0001$. ns, not significant. Abbreviations: ATF4, activating transcription factor 4; GPX4, glutathione peroxidase 4; ACSL4, acyl-CoA synthetase long-chain family member 4; EXO, exosomes; HG, high glucose.

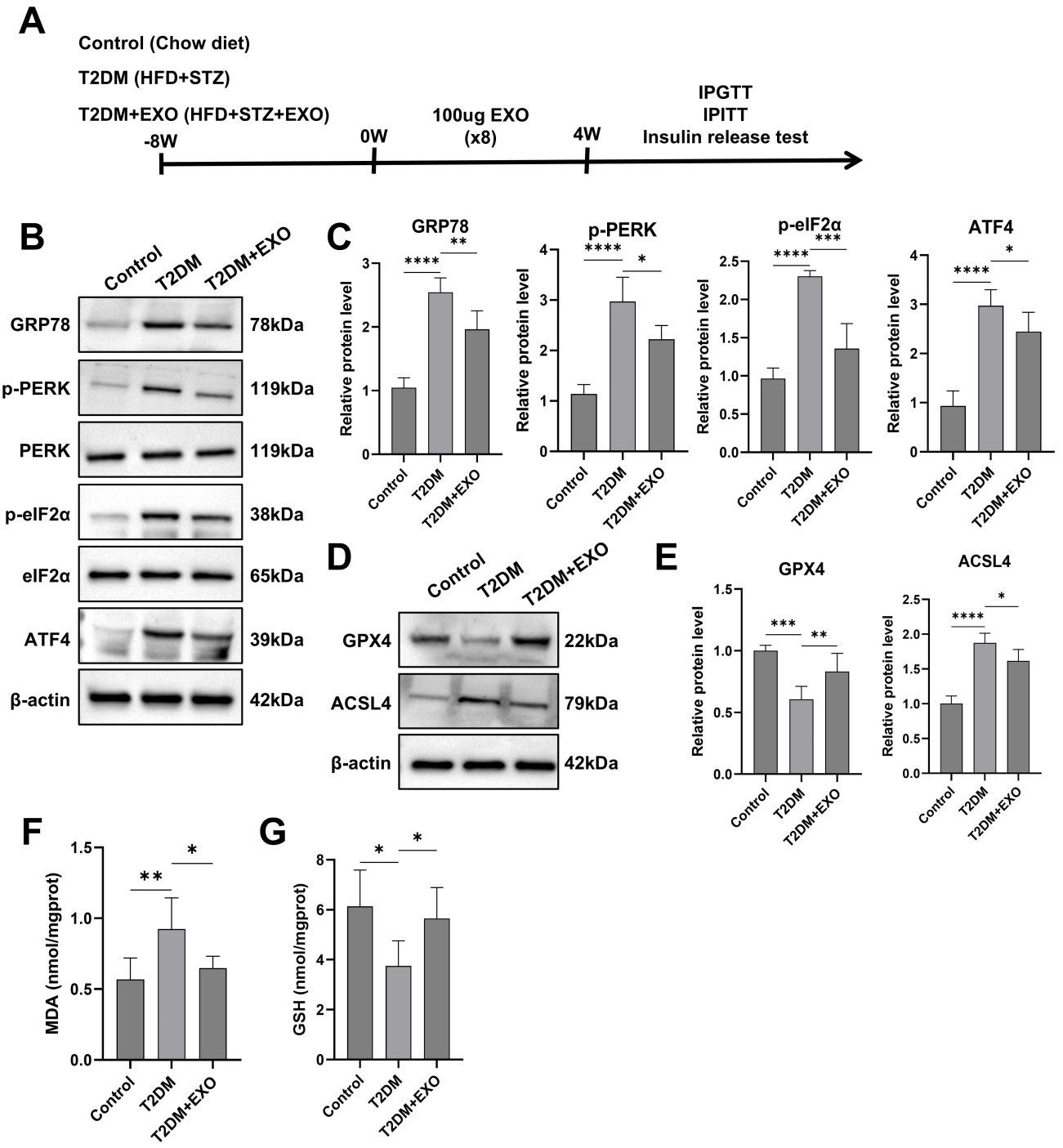

Fig. 5. STC-1-EXO attenuates ER stress and ferroptosis in pancreatic tissues of T2DM mice. (A) Schematic diagram of T2DM mouse model construction. Wild-type mice received HFD for 12 weeks + consecutive 5-day intraperitoneal injection of 60 mg/kg STZ, with STC-1-EXO treatment via tail vein injection during the final 4 weeks, twice weekly, 100 μg STC-1-EXO per treatment, totaling 8 treatments. (B,C) WB analysis of GRP78, p-PERK, p-eIF2α, and ATF4 in pancreatic tissues of T2DM mice (B), with corresponding quantitative analysis (C). (D,E) WB detection of ferroptosis markers GPX4 and ACSL4 in pancreatic tissues of T2DM mice (D), with corresponding quantitative analysis (E). (F,G) MDA and GSH levels in pancreatic tissues of T2DM mice. Data are presented as mean ± SD. n = 6 mice per group. Statistical analysis performed using one-way ANOVA. *$p < 0.05$, **$p < 0.01$, ***$p < 0.001$, ****$p < 0.0001$. Abbreviations: GRP78, glucose-regulated protein 78; p-PERK, phosphorylated-RNA-dependent Protein Kinase-Like ER Kinase; p-eIF2α, phosphorylated eukaryotic translation initiation factor 2α; ATF4, activating transcription factor 4; GPX4, glutathione peroxidase 4; ACSL4, acyl-CoA synthetase long-chain family member 4; MDA, malondialdehyde; GSH, glutathione; EXO, exosomes; HFD, high-fat diet; STZ, streptozotocin; T2DM, type 2 diabetes mellitus; ER, endoplasmic reticulum; ANOVA, analysis of variance.

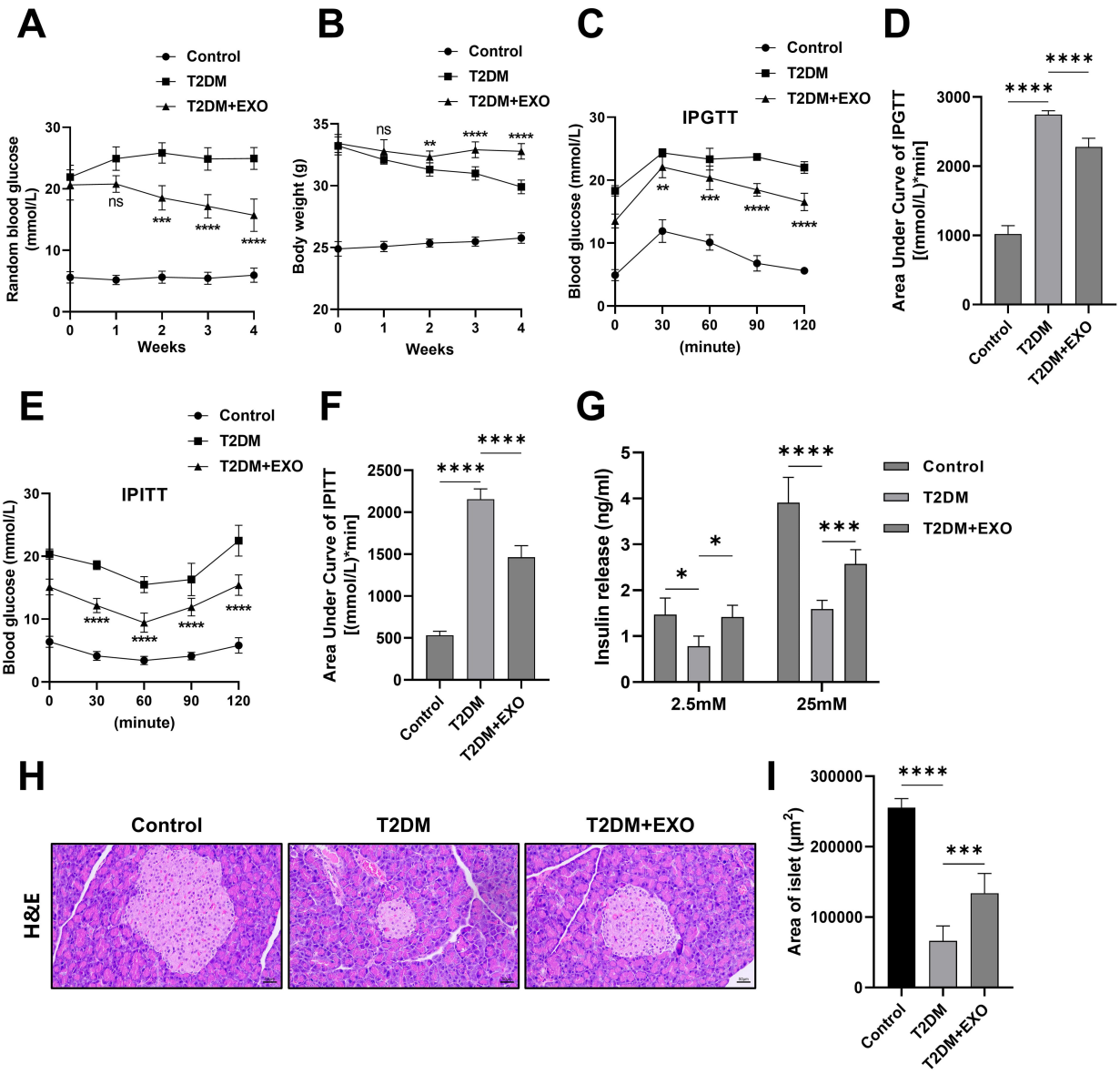

Fig. 6. Early preventive treatment with STC-1-EXO improves β-cell function in T2DM mice. Wild-type mice received HFD for 12 weeks + consecutive 5-day intraperitoneal injection of 60 mg/kg STZ, with STC-1-EXO treatment via tail vein injection during the final 4 weeks, twice weekly, 100 μg STC-1-EXO per treatment, totaling 8 treatments. (A) Random blood glucose levels across experimental groups. (B) Body weight changes across experimental groups over time. (C,D) Mouse blood glucose levels. Following 4-week STC-1-EXO treatment of T2DM mice, IPGTT was performed at week 12. (E,F) Mouse blood glucose levels. Following 4-week STC-1-EXO treatment of T2DM mice, IPITT was performed at week 12. (G) Mouse serum insulin levels. Insulin secretion was detected by ELISA during fasting and 30 minutes post-IPGTT. (H,I) Representative images of pancreatic tissue H&E staining for each group. Scale bar, 50 μm. Data are presented as mean ± SD. n = 6 mice per group. Statistical analysis performed using two-way ANOVA. *$p < 0.05$, **$p < 0.01$, ***$p < 0.001$, ****$p < 0.0001$. ns, not significant. Abbreviations: HFD, high-fat diet; STZ, streptozotocin; T2DM, type 2 diabetes mellitus; IPGTT, intraperitoneal glucose tolerance test; IPITT, intraperitoneal insulin tolerance test; ELISA, Enzyme-Linked Immunosorbent Assay; H&E, Hematoxylin and Eosin Staining.

These results provide further confirmation of STC-1-EXO's protective effects on β-cell function and cellular populations, establishing the therapeutic potential of exosomal intervention in preserving pancreatic β-cell integrity within diabetic pathophysiological contexts.

Discussion

T2DM represents a global chronic metabolic disorder characterized by the fundamental pathophysiological mechanisms of progressive pancreatic β-cell functional deterioration and peripheral tissue insulin resistance. While

conventional hypoglycemic medications demonstrate certain efficacy in glycemic control, the majority fail to fundamentally improve β-cell function and are associated with various adverse effects. In recent years, exosomes have emerged as novel intercellular communication vehicles that, owing to their distinctive nanostructural architecture and enrichment with bioactive molecules, provide new therapeutic approaches for T2DM treatment. This study focuses on STC-1–derived exosomes (EXO), elucidating their inhibitory effects on pancreatic β-cell ferroptosis and underlying mechanistic pathways.

Compared to previous investigations, STC-1-EXO demonstrates distinctive advantages and innovative characteristics. Sun *et al.* [30] demonstrated that human umbilical cord mesenchymal stem cell-derived exosomes (hucMSC-ex) can ameliorate insulin resistance and protect β-cells from damage, primarily through reversing peripheral tissue insulin resistance and alleviating β-cell destruction. In contrast, STC-1-EXO not only significantly improves glycemic levels in T2DM mouse models but also enhances insulin secretory capacity and increases pancreatic β-cell populations through distinctive mechanisms. The unique aspect lies in its precise modulation of the PERK-ATF4 signaling pathway, thereby playing a critical role in alleviating endoplasmic reticulum stress and inhibiting ferroptosis. This mechanistic differentiation provides STC-1-EXO with more direct targeting specificity in regulating pancreatic β-cell function and metabolic environments.

Xia *et al.* [25] demonstrated that modified β-cell-targeting exosomes (Apt-EXO) can enhance pancreatic protection effects, extend blood circulation time, and further improve β-cell function and numbers. In comparison, STC-1-EXO, as a component of the gastrointestinal endocrine system, possesses the advantage of more intimate physiological connections with pancreatic β-cells, enabling regulation of gut-pancreas axis function. The specialized anatomical position and functional characteristics of STC-1 cells within the gastrointestinal tract allow STC-1-EXO to more directly influence pancreatic β-cell function. This physiologically-based regulatory mechanism provides more targeted strategies for diabetes treatment, expanding the therapeutic applications of exosomes in diabetic management.

Furthermore, the discovery of STC-1-EXO contributes to expanding our understanding of exosomal functionality. Exosomes function not only as intercellular communication carriers but also precisely regulate specific signaling pathways through their bioactive molecular cargo, thereby playing important roles in disease treatment. The innovative discovery of STC-1-EXO's ferroptosis inhibitory properties provides new insights for precision medicine based on intercellular communication. This precise regulatory capacity positions STC-1-EXO as a potential clinical therapeutic intervention with promise for development as an innovative treatment modality.

At the mechanistic level, this study innovatively reveals that STC-1-EXO attenuates endoplasmic reticulum (ER) stress through inhibition of the PERK-ATF4 signaling pathway, subsequently suppressing ferroptosis. Previous research has clearly established the critical role of ER stress in diabetic β-cell damage. Ali *et al.* [31] demonstrated that PERK pathway activation occurs during protein misfolding events, triggering cellular apoptosis. Stockwell [32] proposed ferroptosis as a novel cell death modality closely associated with intracellular ER stress, iron metabolism dysregulation, and intensified lipid peroxidation reactions. Our experimental results demonstrate high concordance with these foundational theoretical frameworks, further refining the specific targeting mechanisms of exosomes in regulating ER stress and ferroptosis.

Unlike the mechanism reported by Xia *et al.* [25], wherein MSC-EXO inhibits ferroptosis through AKT/ERK signaling pathway-mediated NRF2 regulation, STC-1-EXO primarily targets the PERK-ATF4 pathway. This mechanistic differentiation may be attributable to STC-1 cells' specialized environmental adaptation within the gastrointestinal tract for precise pancreatic β-cell regulation, reflecting the mechanistic diversity among different exosomal types. STC-1-EXO effectively inhibits ferroptosis through PERK-ATF4 pathway suppression, reducing GRP78, p-PERK, p-eIF2α, and ATF4 expression while simultaneously decreasing ACSL4 expression and enhancing GPX4 expression. This mechanistic discovery not only provides new perspectives for understanding exosomal roles in diabetic treatment but also establishes theoretical foundations for developing PERK-ATF4 pathway-targeted therapeutic approaches.

This study validates ATF4's importance in STC-1-EXO's anti-ferroptotic effects through lentivirus-mediated ATF4 overexpression experiments. Our findings demonstrate that ATF4 overexpression significantly attenuates STC-1-EXO's regulatory effects on ACSL4 and GPX4 expression as well as its inhibitory effects on lipid peroxidation product accumulation. This provides direct evidence supporting STC-1-EXO's anti-ferroptotic effects through ATF4 inhibition. Additionally, STC-1-EXO demonstrates significant protective effects in both *in vitro* and *in vivo* experiments [18], further confirming mechanistic consistency and providing robust support for its potential as a therapeutic intervention.

The innovative discovery of STC-1-EXO's ferroptosis inhibitory mechanisms further enriches our understanding of exosomal functionality. Exosomes serve not only as intercellular communication carriers but also precisely regulate specific signaling pathways through their bioactive molecular cargo, thereby playing important roles in disease treatment. STC-1-EXO not only inhibits ferroptosis through PERK-ATF4 pathway modulation but also significantly improves pancreatic β-cell function and populations. This precise regulatory capacity positions STC-1-EXO with

potential clinical therapeutic value and promise for development as an innovative treatment modality.

Integrating previous research findings, the discovery of STC-1-EXO provides new perspectives for T2DM treatment. Kalluri *et al*. [33,34] indicate that exosomes' roles in intercellular communication make them ideal therapeutic carriers, with their low immunogenicity and high stability providing foundations for clinical applications. While this study validates STC-1-EXO's efficacy in animal models, clinical translation requires addressing critical challenges including standardized exosomal extraction protocols, large-scale production, and quality control systems. Furthermore, preclinical studies should evaluate STC-1-EXO's long-term efficacy and safety profiles across different diabetic models to validate its potential as a novel therapeutic agent.

Undeniably, while this study provides new mechanisms and targets for STC-1-EXO in T2DM treatment, certain limitations remain. Firstly, this research primarily focuses on *in vitro* cellular experiments and animal models, lacking clinical sample validation. Future investigations should further validate STC-1-EXO's therapeutic effects and mechanisms in diabetic patients. Secondly, the specific bioactive molecules within STC-1-EXO responsible for protective effects remain incompletely characterized, requiring future application of advanced technologies such as proteomics for component isolation and identification. Additionally, while this study primarily examines the PERK-ATF4 pathway's role in STC-1-EXO's antiferroptotic effects, other potential signaling pathways (such as NRF2, p38 MAPK) may also participate, warranting further investigation.

Conclusion

In summary, this study systematically investigated the therapeutic effects of STC-1-EXO on T2DM and its underlying mechanisms through comprehensive *in vitro* and *in vivo* experimental approaches. Our findings demonstrate that STC-1-EXO significantly improves glycemic levels in T2DM mouse models, enhances insulin secretory capacity, and increases pancreatic β-cell populations. The primary mechanistic pathway involves inhibition of the PERK-ATF4 signaling cascade, attenuation of endoplasmic reticulum stress, and subsequent suppression of ferroptosis. This discovery expands the therapeutic applications of STC-1-EXO in diabetic treatment and provides new insights for precision medicine based on intercellular communication. Future research should further explore STC-1-EXO's therapeutic efficacy and safety profiles in human subjects, while developing more efficient exosomal extraction and delivery technologies to advance clinical translation and potentially establish it as a clinically applicable innovative therapeutic modality.

Availability of Data and Materials

The datasets generated and analyzed during the current study are included within this published article. Raw data supporting the conclusions of this article are available from the corresponding author upon reasonable request.

Author Contributions

XZ conceptualized and designed the research framework and experimental methodology. XC and LH conducted the experimental procedures, performed data acquisition, and executed statistical analyses. XC, LH, and XZ contributed to manuscript drafting and critical revision. All authors have reviewed and approved the final version of the manuscript. All authors have participated sufficiently in the work to take public responsibility for appropriate portions of the content and agreed to be accountable for all aspects of the work in ensuring that questions related to its accuracy or integrity.

Ethics Approval and Consent to Participate

All protocols were approval by the Institutional Animal Care and Use Committee of Nantong University (Approval Number: P20230321-018) and conducted in accordance with National Institutes of Health (NIH) guidelines.

Acknowledgment

Not applicable.

Funding

This research was supported by the General Research Project (Directive) of Nantong Municipal Health Commission (Grant No. MS2022072).

Conflict of Interest

The authors declare no conflict of interest.

Supplementary Material

Supplementary material associated with this article can be found, in the online version, at https://doi.org/10.24976/Discov.Med.202638206.59.

References

[1] Strati M, Moustaki M, Psaltopoulou T, Vryonidou A, Paschou SA. Early onset type 2 diabetes mellitus: an update. Endocrine. 2024; 85: 965–978. https://doi.org/10.1007/s12020-024-03772-w.

[2] Tinajero MG, Malik VS. An Update on the Epidemiology of Type 2 Diabetes: A Global Perspective. Endocrinology and Metabolism Clinics of North America. 2021; 50: 337–355. https://doi.org/10.1016/j.ecl.2021.05.013.

[3] Młynarska E, Czarnik W, Dzieża N, Jędraszak W, Majchrowicz G, Prusinowski F, *et al*. Type 2 Diabetes Mellitus: New Pathogenetic Mechanisms, Treatment and the Most Important Complications. International Journal of Molecular Sciences. 2025; 26: 1094. https://doi.org/10.3390/ijms26031094.

[4] Singh A, Shadangi S, Gupta PK, Rana S. Type 2 Diabetes Mellitus: A Comprehensive Review of Pathophysiology, Comorbidities, and Emerging Therapies. Comprehensive Physiology. 2025; 15: e70003. https://doi.org/10.1002/cph4.70003.

[5] Wang S, Li S. Type 2 diabetes, heart failure and the treatment of their comorbidity. Minerva Medica. 2025; 116: 141–155. https://doi.org/10.23736/S0026-4806.24.09264-4.

[6] Lee Jia Jia I, Zampetti S, Pozzilli P, Buzzetti R. Type 2 diabetes in children and adolescents: Challenges for treatment and potential solutions. Diabetes Research and Clinical Practice. 2024; 217: 111879. https://doi.org/10.1016/j.diabres.2024.111879.

[7] Shan SK, Lin X, Wu F, Li CC, Guo B, Li FXZ, *et al*. Vascular wall microenvironment: Endothelial cells original exosomes mediated melatonin-suppressed vascular calcification and vascular ageing in a m6A methylation dependent manner. Bioactive Materials. 2024; 42: 52–67. https://doi.org/10.1016/j.bioactmat.2024.08.021.

[8] Wang X, Tian R, Liang C, Jia Y, Zhao L, Xie Q, *et al*. Biomimetic nanoplatform with microbiome modulation and antioxidant functions ameliorating insulin resistance and pancreatic β-cell dysfunction for T2DM management. Biomaterials. 2025; 313: 122804. https://doi.org/10.1016/j.biomaterials.2024.122804.

[9] Yang S, Yuan Y, Zhang B, Wu T, Yu C, Li F, *et al*. Identification of adipose tissue-derived exosomal microRNA as a novel causal biomarker for cognitive impairment in type 2 diabetes mellitus: Triangulating evidence from Mendelian randomization and multicentre population studies. Diabetes, Obesity & Metabolism. 2025; 27: 1265–1275. https://doi.org/10.1111/dom.16121.

[10] Zou J, Song Q, Shaw PC, Wu Y, Zuo Z, Yu R. Tangerine Peel-Derived Exosome-Like Nanovesicles Alleviate Hepatic Steatosis Induced by Type 2 Diabetes: Evidenced by Regulating Lipid Metabolism and Intestinal Microflora. International Journal of Nanomedicine. 2024; 19: 10023–10043. https://doi.org/10.2147/IJN.S478589.

[11] Aswani BS, Hegde M, Vishwa R, Alqahtani MS, Abbas M, Almubarak HA, *et al*. Tackling exosome and nuclear receptor interaction: an emerging paradigm in the treatment of chronic diseases. Military Medical Research. 2024; 11: 67. https://doi.org/10.1186/s40779-024-00564-1.

[12] Gao C, Chen Y, Wen X, Han R, Qin Y, Li S, *et al*. Plant-derived exosome-like nanoparticles in tissue repair and regeneration. Journal of Materials Chemistry. B. 2025; 13: 2254–2271. https://doi.org/10.1039/d4tb02394c.

[13] Saleem M, Shahzad KA, Marryum M, Singh S, Zhou Q, Du S, *et al*. Exosome-based therapies for inflammatory disorders: a review of recent advances. Stem Cell Research & Therapy. 2024; 15: 477. https://doi.org/10.1186/s13287-024-04107-2.

[14] Lee E, Ryu GR, Moon SD, Ko SH, Ahn YB, Song KH. Reprogramming of enteroendocrine K cells to pancreatic β-cells through the combined expression of Nkx6.1 and Neurogenin3, and reaggregation in suspension culture. Biochemical and Biophysical Research Communications. 2014; 443: 1021–1027. https://doi.org/10.1016/j.bbrc.2013.12.093.

[15] Li P, Zhu L, Yang X, Li W, Sun X, Yi B, *et al*. Farnesoid X receptor interacts with cAMP response element binding protein to modulate glucagon-like peptide-1 (7-36) amide secretion by intestinal L cell. Journal of Cellular Physiology. 2019; 234: 12839–12846. https://doi.org/10.1002/jcp.27940.

[16] Lin LC, Lee LC, Huang C, Chen CT, Song JS, Shiao YJ, *et al*. Effects of boschnaloside from Boschniakia rossica on dysglycemia and islet dysfunction in severely diabetic mice through modulating the action of glucagon-like peptide-1. Phytomedicine: International Journal of Phytotherapy and Phytopharmacology. 2019; 62: 152946. https://doi.org/10.1016/j.phymed.2019.152946.

[17] Han J, Lee HH, Kwon H, Shin S, Yoon JW, Jun HS. Engineered enteroendocrine cells secrete insulin in response to glucose and reverse hyperglycemia in diabetic mice. Molecular Therapy: the Journal of the American Society of Gene Therapy. 2007; 15: 1195–1202. https://doi.org/10.1038/sj.mt.6300117.

[18] Yang S, Cao J, Wang Y, Chen Q, Li F, Gao Y, *et al*. Small Intestinal Endocrine Cell Derived Exosomal ACE2 Protects Islet β-Cell Function by Inhibiting the Activation of NLRP3 Inflammasome and Reducing β-Cell Pyroptosis. International Journal of Nanomedicine. 2024; 19: 4957–4976. https://doi.org/10.2147/IJN.S450337.

[19] Chen X, Shi C, He M, Xiong S, Xia X. Endoplasmic reticulum stress: molecular mechanism and therapeutic targets. Signal Transduction and Targeted Therapy. 2023; 8: 352. https://doi.org/10.1038/s41392-023-01570-w.

[20] Hetz C. The unfolded protein response: controlling cell fate decisions under ER stress and beyond. Nature Reviews. Molecular Cell Biology. 2012; 13: 89–102. https://doi.org/10.1038/nrm3270.

[21] Prasad M K, Mohandas S, Ramkumar KM. Role of ER stress inhibitors in the management of diabetes. European Journal of Pharmacology. 2022; 922: 174893. https://doi.org/10.1016/j.ejphar.2022.174893.

[22] Tang H, Kang R, Liu J, Tang D. ATF4 in cellular stress, ferroptosis, and cancer. Archives of Toxicology. 2024; 98: 1025–1041. https://doi.org/10.1007/s00204-024-03681-x.

[23] Sha W, Hu F, Xi Y, Chu Y, Bu S. Mechanism of Ferroptosis and Its Role in Type 2 Diabetes Mellitus. Journal of Diabetes Research. 2021; 2021: 9999612. https://doi.org/10.1155/2021/9999612.

[24] Deng L, Mo MQ, Zhong J, Li Z, Li G, Liang Y. Iron overload induces islet β cell ferroptosis by activating ASK1/P-P38/CHOP signaling pathway. PeerJ. 2023; 11: e15206. https://doi.org/10.7717/peerj.15206.

[25] Xia L, Yang M, Zang N, Song J, Chen J, Hu H, *et al*. PEGylated β-Cell-Targeting Exosomes from Mesenchymal Stem Cells Improve β Cell Function and Quantity by Suppressing NRF2-Mediated Ferroptosis. International Journal of Nanomedicine. 2024; 19: 9575–9596. https://doi.org/10.2147/IJN.S459077.

[26] Hu H, Zhao R, He Q, Cui C, Song J, Guo X, *et al*. cGAS-STING mediates cytoplasmic mitochondrial-DNA-induced inflammatory signal transduction during accelerated senescence of pancreatic β-cells induced by metabolic stress. FASEB Journal: Official Publication of the Federation of American Societies for Experimental Biology. 2022; 36: e22266. https://doi.org/10.1096/fj.202101988R.

[27] Guo T, Yan W, Cui X, Liu N, Wei X, Sun Y, *et al*. Liraglutide attenuates type 2 diabetes mellitus-associated non-alcoholic fatty liver disease by activating AMPK/ACC signaling and inhibiting ferroptosis. Molecular Medicine (Cambridge, Mass.). 2023; 29: 132. https://doi.org/10.1186/s10020-023-00721-7.

[28] Huang Q, Tian L, Zhang Y, Qiu Z, Lei S, Xia ZY. Nobiletin alleviates myocardial ischemia-reperfusion injury via ferroptosis in rats with type-2 diabetes mellitus. Biomedicine & Pharmacotherapy. 2023; 163: 114795. https://doi.org/10.1016/j.biopha.2023.114795.

[29] Zhao Y, Guo H, Li Q, Wang N, Yan C, Zhang S, *et al*. TREM1 induces microglial ferroptosis through the PERK pathway in diabetic-associated cognitive impairment. Experimental Neurology. 2025; 383: 115031. https://doi.org/10.1016/j.expneurol.2024.115031.

[30] Sun Y, Shi H, Yin S, Ji C, Zhang X, Zhang B, *et al*. Human Mesenchymal Stem Cell Derived Exosomes Alleviate Type 2 Diabetes Mellitus by Reversing Peripheral Insulin Resistance and Relieving β-Cell Destruction. ACS Nano. 2018; 12: 7613–7628. https://doi.org/10.1021/acsnano.7b07643.

[31] Ali T, Lei X, Barbour SE, Koizumi A, Chalfant CE, Ramanadham S. Alterations in β-Cell Sphingolipid Profile Associated with ER Stress and iPLA$_2\beta$: Another Contributor to β-Cell Apoptosis in Type 1 Diabetes. Molecules (Basel, Switzerland). 2021; 26: 6361. https://doi.org/10.3390/molecules26216361.

[32] Stockwell BR. Ferroptosis turns 10: Emerging mechanisms, physiological functions, and therapeutic applications. Cell. 2022; 185: 2401–2421. https://doi.org/10.1016/j.cell.2022.06.003.

[33] Kalluri R. The biology and function of extracellular vesicles in immune response and immunity. Immunity. 2024; 57: 1752–1768. https://doi.org/10.1016/j.immuni.2024.07.009.

[34] Kalluri R, McAndrews KM. The role of extracellular vesicles in cancer. Cell. 2023; 186: 1610–1626. https://doi.org/10.1016/j.cell.2023.03.010.